Production, Characterization, and Utilization of Aerosol-Deposited Sol−Gel-Derived Films

Jeffrey D. Jordan, Richard A. Dunbar, Daniel J. Hook, Hengzhong Zhuang, Joseph A. Gardella, Jr., Luis A. Colón, and Frank V. Bright*

Department of Chemistry, Natural Sciences Complex, State University of New York at Buffalo, Buffalo, New York 14260-3000

Received September 10, 1997. Revised Manuscript Received December 9, 1997

A new aerosol-based deposition method, for the production of sol−gel-derived films under ambient conditions, has been developed. Tetraethyl orthosilicate (TEOS) and *N*-octyltriethoxysilane (TrEOS-C_8)-derived sol−gel-processed films were produced using the new technique and compared to films produced by a conventional spin-casting approach. All films were characterized using scanning electron microscopy, profilometry, electron spectroscopy for chemical analysis (ESCA), diffuse-reflectance infrared Fourier transform spectroscopy, and steady-state fluorescence spectroscopy. Sol−gel-derived films produced using the aerosol-based method were uniform, and their thickness could be controlled between 0.6 and at least 3.0 μm. Spin casting of the neat sol−gel-processed solutions generally yielded more thick (2.0 ± 0.10 μm) films, but these thicker films were of poorer optical quality and very often more highly cracked. ESCA data demonstrate surface segregation of the C_8 moiety within the TrEOS−C_8-derived films. This segregation phenomenon is much more pronounced in the aerosol-generated films. A scenario is proposed where the distribution of and/or the dynamics/solvation of the C_8 residue within the aerosol droplet vs the bulk cast film are very different and lead to the segregation. Static fluorescence experiments demonstrate that several dopant classes can be incorporated directly into the sol−gel-processed solution and aerosol deposited. All results are also consistent with films that are heterogeneous on a molecular level. The utility of aerosol-deposited, sol−gel-derived films as a chemical sensing platform is demonstrated using fluorescence quenching of entrapped pyrene by O_2.

Introduction

Sol−gel processing allows one to produce porous glasses under ambient conditions.[1−6] The mild preparation conditions offer an opportunity for researchers to incorporate a wide range of labile organic species into a glass composite.[1−6] In addition to the mild processing conditions, sol−gel-derived materials exhibit tunable porosity, good thermal stability, good optical transparency, and the basic preparation method is reasonably simple.[1−6] To date, sol−gel processing has largely been used to develop advanced optical coatings, solid-state lasers and lasing materials, and electrooptic materials.[1−5] More recently, several research groups have focused on entrapping recognition chemistry within sol−gel-processed materials for sensing applications.[6−18] Sol−gel processing has also been used to form stable chromatographic stationary phase.[19]

Early sol−gel-derived sensors were based on recognition chemistries that were entrapped within porous glass *monoliths*. Although these platforms functioned as intended, they generally exhibited slow response times that were associated with long analyte diffusion pathways within the monolith. The slow response time can be most easily addressed by using film-based sensor platforms. Sol−gel-derived films are commonly pre-

(1) *Chemical Processing of Advanced Materials*; Hench, L. L., West, J. K., Eds.; Wiley: New York, 1992.
(2) Hench, L. L.; West, J. K. *Chem. Rev.* **1990**, *90*, 33.
(3) Brinker, C. J.; Scherer, G. W. *Sol−Gel Science*; Academic Press: New York, 1989.
(4) *Sol−Gel Optics: Processing and Applications*; Klein, L. C., Ed.; Kluwer Academic: Boston, 1994.
(5) Avnir, D.; Braun, S.; Lev, O.; Ottolenghi, M. *SPIE Sol−Gel Opt. II* **1992**, *1758*, 546.
(6) Ingersoll, C. M.; Bright, F. V. *CHEMTECH* **1997**, *27*, 26.
(7) Narang, U.; Dunbar, R. A.; Bright, F. V.; Prasad, P. N. *Appl. Spectrosc.* **1993**, *47*, 1700.
(8) (a) Narang, U.; Prasad, P. N.; Bright, F. V.; Kumar, A.; Kumar, N. D.; Malhotra, B. D.; Kamalasanan, M. N.; Chandra, S. *Anal. Chem.* **1994**, *66*, 3139. (b) Narang, U.; Prasad, P. N.; Bright, F. V.; Kumar, A.; Kumar, N. D.; Malhotra, B. D.; Kamalasanan, M. N.; Chandra, S. *Chem. Mater.* **1994**, *6*, 1596.
(9) Ellerby, L.; Nishida, C. R.; Nishida, R.; Yamanaka, S. A.; Dunn, B.; Valentine, J. S.; Zink, J. I. *Science* **1992**, *255*, 1113.
(10) Shtelzer, S.; Rappoport, S.; Avnir, D.; Ottolenghi, M.; Braun, S. *Biotechnol. Appl. Biochem.* **1992**, *15*, 227.
(11) Avnir, D.; Braun, S.; Ottolenghi, M. In *Supramolecular Architecture*; Bein, T., Ed.; American Chemical Society: Washington, 1992; Vol. 499.
(12) Wang, R.; Narang, U.; Prasad, P. N.; Bright, F. V. *Anal. Chem.* **1993**, *65*, 2671.
(13) Dave, B. C.; Dunn, B.; Valentine, J. S.; Zink, J. I. *Anal. Chem.* **1994**, *66*, 1120A.
(14) Edmiston, P. L.; Wambolt, C. L.; Smith, M. K.; Saavedra, S. S. *J. Colloid Interface Sci.* **1994**, *163*, 395.
(15) Jordan, J. D.; Dunbar, R. A.; Bright, F. V. *Anal. Chem.* **1995**, *67*, 2436.
(16) Narang, U.; Rahman, M. H.; Wang, J. H.; Prasad, P. N.; Bright, F. V. *Anal. Chem.* **1995**, *67*, 1935.
(17) Lev, O.; Tsionsky, M.; Rabinovich, L.; Glezer, V.; Sampath, S.; Pankratov, I.; Gun, J. *Anal. Chem.* **1995**, *67*, 22A.
(18) Hinz, P.; Dislich, H. *J. Non-Cryst. Solids* **1986**, *82*, 411.
(19) (a) Guo, Y.; Colón, L. A. *Anal. Chem.* **1995**, *67*, 2511. (b) Wang, D.; Chong, S. L.; Malik, A. *Anal. Chem.* **1997**, *69*, 4566.

S0897-4756(97)00612-1 CCC: $15.00
Published on Web 02/19/1998

pared by dip- or spin-coating methods.[4,5] Unfortunately, these approaches are wasteful because a substantial fraction of any dopant (i.e., recognition chemistry) and the sol−gel processing solution are not actually incorporated into the final film.

Alternative film formation methods include spraying,[18] electrophoresis,[20] thermophoresis,[21] and ultrasonication.[22−24] Joubert and co-workers[22−24] reported an ultrasonication method to produce a sol−gel-processed solution aerosol that was transported by a carrier gas to a temperature-controlled substrate. By using this apparatus and adjusting the tetraethyl orthosilicate (TEOS)-to-water molar ratio, solution viscosity, and deposition time the authors produced 0.20 ± 0.02 μm thick films. These films were characterized by FT-IR, profilometry, and refractive index measurement; however, most of these films were also studied *after* they were processed at several hundred degrees. Unfortunately, few, if any, biorecognition chemistries will remain viable after such high-temperature processing.

Jordan et al.[25] recently reported on a simple, inexpensive aerosol generation device for producing sol−gel-derived films at ambient conditions. In this particular work, an antibody sensing layer was entrapped between two aerosol-generated, sol−gel-processed films. The entrapped antibody remained functional for many weeks, and the sensing platform could be easily reused/reset. The attractions of this approach are that it yielded a stable biosensor platform, resulted in near zero waste of the expensive antibody, and the method could be used to coat films on irregular substrates.[25,26]

In the current paper, we aim to characterize and compare a series of sol−gel-derived films that are prepared using our aerosol deposition technique to films that are produced using a conventional spin-coating method. In each case the exact same sol−gel processing solution is used to prepare the films for study. Tetraethyl orthosilicate (TEOS) and an organically modified silane (ORMOSIL), *N*-octyltriethoxysilane (TrEOS−C_8), are used as the precursors. TEOS was chosen because it is among the most common precursors used in sol−gel science and technology.[1−5] TrEOS−C_8 is used because previous work by Guo and Colón[19a] has shown the utility of this particular precursor to form reliable chromatographic stationary phases. Cationic (rhodamine 6G), anionic (fluorescein), and neutral (pyrene) fluorophores were used as model dopants and serve also to report on the average microenvironment surrounding a dopant entrapped within these sol−gel-processed films. Surface-adsorbed pyrene is also used to report on the average "dipolarity" at the film surfaces. Films are also characterized by scanning electron microscopy (SEM), profilometry, electron spectroscopy for chemical analysis (ESCA), and diffuse reflectance infrared Fourier transform spectroscopy (DRIFTS). We also report on the performance of the aerosol-deposited films for chemical sensing.

Experimental Section

Reagents. The following chemicals were used: tetraethyl orthosilicate (TEOS) and *N*-octyltriethoxysilane (TrEOS−C_8) (United Chemical Technologies), rhodamine 6G (R6G), fluorescein, and pyrene (Aldrich), ethanol (200 proof, Quantum Chemical), Na_2HPO_4, $NaH_2PO_4{\cdot}2H_2O$, KOH, and HCl (Fisher), and nitrogen (99% bone dry), and argon (99%) (Scott). All reagents were used as received without further purification. All aqueous solutions were prepared by using distilled, deionized water.

Preparation of Sol−Gel Processed Stock Solutions. Sol−gel-processed stock solutions were prepared using TEOS, ethanol, water and HCl in the molar ratios 1:2:2:10^{-5} or 1:2:4:10^{-5}. The organically modified silane (ORMOSIL) stock solution was prepared by using TrEOS−C_8, ethanol, water, and HCl in the molar ratio 1:2:3:10^{-4}. In all solutions, processing was initiated by mixing the alkoxide and ethanol in an Erlenmeyer flask for 1 min. In a second step, the water/HCl mixture was added dropwise to the alkoxide/ethanol solution under constant stirring at 20−22 °C. The stock solution was then sealed and allowed to stir/hydrolyze. After mixing for 24 h under the aforementioned conditions, the stock solutions were used to prepare films.

Sample Film Generation. Borosilicate glass microscope slides (1 × 1 cm) or quartz plates (1 × 1 cm) were used as the primary substrates for all film deposition. Prior to film coating, the substrates were soaked overnight in aqueous 1 M KOH, rinsed with copious amounts of distilled−deionized water, and dried at 40 °C. The substrates to be coated were loaded into an argon-purged glovebag, and films were deposited (at 20−22 °C) by spin casting or aerosol deposition (vide infra). During the actual film formation, the spin coater and the aerosol deposition unit were housed fully within the same argon-purged bag at all times. Once the films were formed, they remained in the argon atmosphere for 1−2 h for initial curing. After this period most films/substrates were transferred to a covered Petri dish to effect aging. In some cases, the films were maintained in an inert argon atmosphere while they aged.

For the fluorescence experiments, the TEOS-derived sol−gel-processed stock solutions were doped (just prior to film generation) with R6G, fluorescein, or pyrene such that the final fluorophore concentration in the stock solution was 1 μM.

Adsorbed fluorophore studies were carried out by incubating sol−gel-processed films in 0.5 μM pyrene solution (in ethanol) for 1 h. Films were subsequently removed from the pyrene solution, rinsed with ethanol, and allowed to air-dry.

Spin Casting. The glass/quartz substrate was affixed within a home-built rotor, and 200−300 μL of the appropriate (neat or fluorophore-doped) sol−gel processing solution was pipetted directly onto the center of the substrate. Once the sol−gel-processed sample was pipetted onto the substrate, the substrate was immediately spun at 2000 rpm for 15 s to form the film. The film was then allowed the sit for 5−6 min and then was removed from the rotor.

Aerosol Application. The apparatus used to produce the aerosol-deposited films has been described previously.[25] Briefly, the system consists of an ultrasonic humidifier (Holmes, Model number HM-460B) and an inverted 250 mL Erlenmeyer flask. The flask has a Pyrex inlet for N_2 gas/sol−gel-processed solution loading and an outlet for transporting the aerosol to the substrate. A 0.001 in. thick poly(tetrafluoroethylene cohexafluoropropylene) (FEP) membrane is affixed over the flask mouth. This membrane serves to seal the flask and provides a means to couple the ultrasonic energy from the transducer into the sol−gel-processed solution. The flask is mounted such that the FEP film/flask mouth is approximately

(20) Clark, D. E.; Datzell, W. J.; Folz, D. C. *Ceram. Eng. Sci. Proc.* **1988**, *9*, 111.
(21) Derjaguin, B.; Rabinovich, Y. I.; Storozhilova, A. I.; Shcherbing, G. I. *J. Colloid Interface Sci.* **1976**, *57*, 451.
(22) Marage, P.; Langlet, M.; Joubert, J. C. *Thin Solid Films* **1994**, *238*, 218.
(23) Langlet, M.; Walz, D.; Marage, P.; Joubert, J. C. *Thin Solid Films* **1992**, *221*, 44.
(24) Langlet, M.; Walz, D.; Marage, P.; Joubert, J. C. *J. Non-Cryst. Solids* **1992**, *147 & 148*, 488.
(25) Jordan, J. D.; Dunbar, R. A.; Bright, F. V. *Anal. Chim. Acta* **1996**, *332*, 83.
(26) Jordan, J. D.; Grinstead, K. D.; Gord, J. R.; Weaver, W. L.; Trump, D. D.; Gruber, M. R.; Goss, L. P.; Bright, F. V. *Appl. Spectrosc.*, submitted for publication.

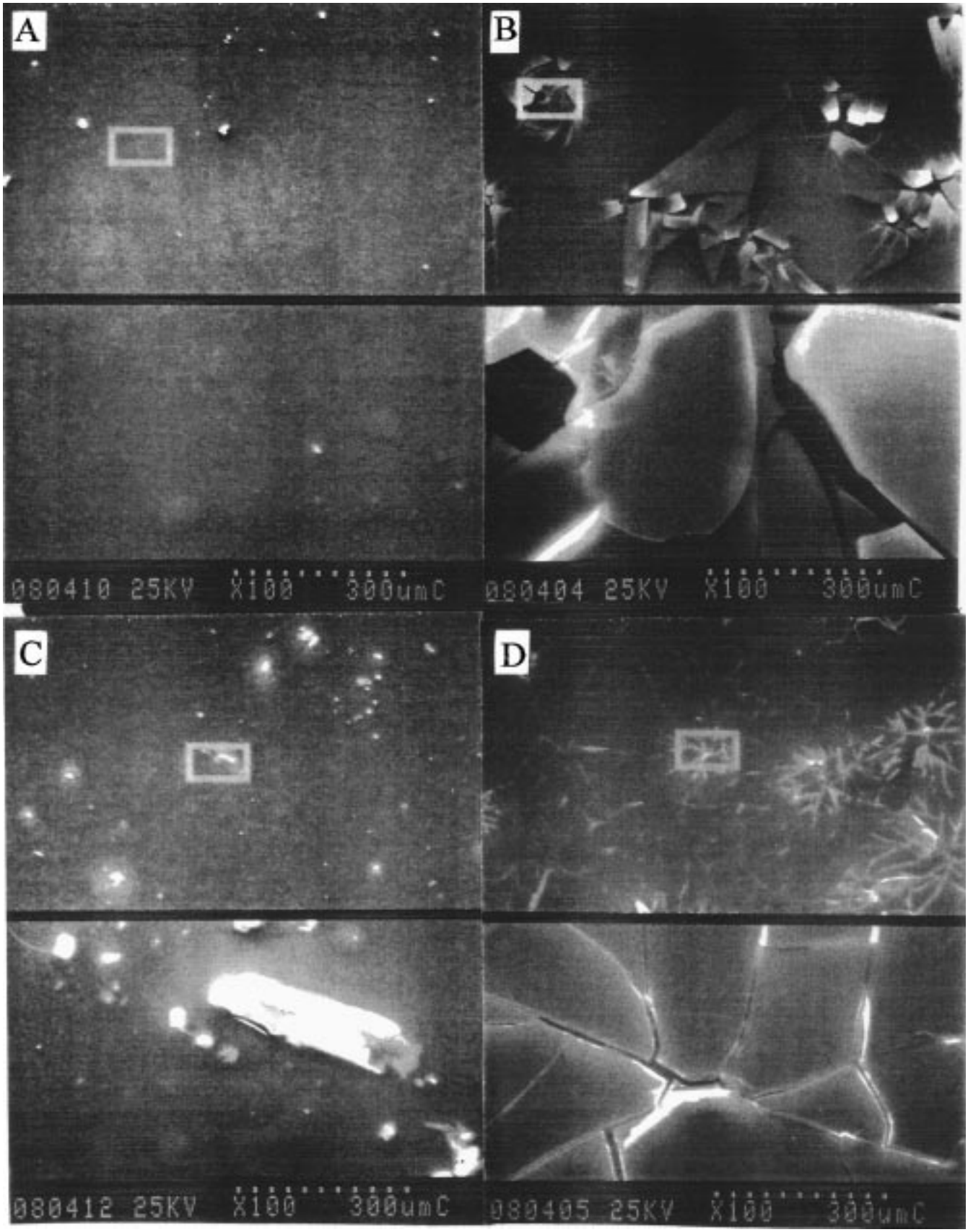

Figure 1. Scanning electron micrographs (100× magnification (upper images), 1000× magnification (lower images)) of TEOS-derived aerosol-generated (A, C) and spin-cast (B, D) thin films. (A, B) Molar ratio of TEOS:ethanol:water:HCl 1:2:2:10^{-5}. (C, D) Molar ratio of TEOS:ethanol:water:HCl 1:2:4:10^{-5}. The 300 μm scale corresponds to the upper image within each panel pair. The same scale represents 30 μm in the lower image of each panel pair.

1 cm above the ultrasonic transducer. A 2 mL aliquot of a particular sol−gel-processed stock solution is introduced into the flask through the N_2 exit port using a disposable Pasteur pipet. In operation, the ultrasonic humidifier is engaged and

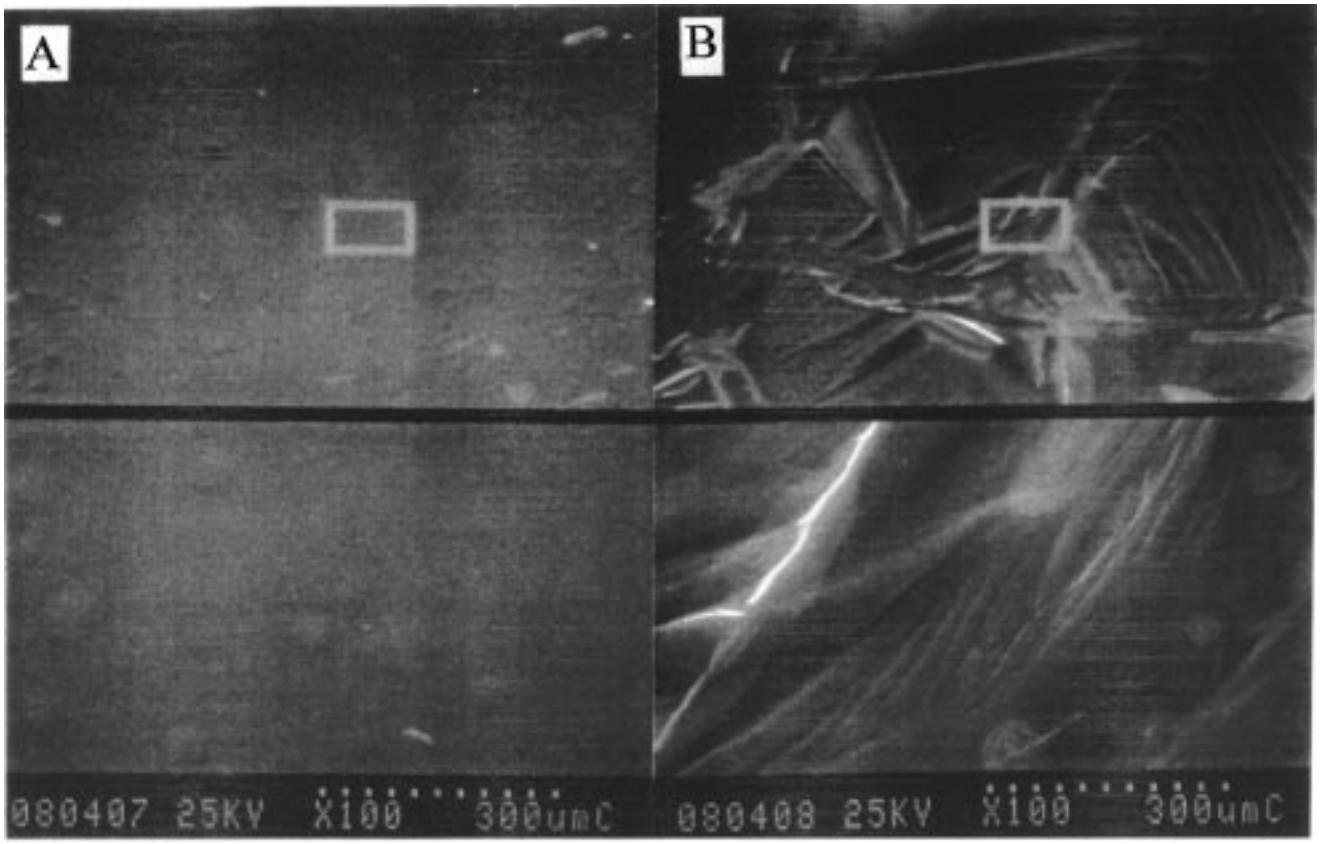

Figure 2. Scanning electron micrographs (100× magnification (upper), 1000× magnification (lower)) of TrEOS−C_8-derived aerosol-generated (A) and spin-cast (B) thin films. The 300 μm scale corresponds to the upper image within each panel pair. The same scale represents 30 μm in the lower image of each panel pair.

a visible mist forms within the vessel. After a few seconds, the N_2 flow is initiated (0.5 mL/s), the mist is transported to the primary substrate via $^1/_4$ in. (i.d.) Tygon tubing, and guided toward the glass slide using a Pasteur pipet. The sol−gel-derived aerosol is distributed over the substrate by manually translating the pipet tip in a sweeping motion. In certain instances multiple films were overcoated one atop the other.

We do not know the distribution of the aerosol droplet sizes, but we suspect they are in the micron-to-submicron range because we can see them visually.

Film Aging. All films were preaged in the argon atmosphere for 1−2 h after preparation. In most cases the films were carefully removed from the argon atmosphere and aged at 20−22 °C in air for 1−3 weeks prior to analysis. In a few cases, films were maintained continuously in the argon atmosphere while they aged.

Film Characterization. *Scanning Electron Microscopy (SEM).* SEM images were obtained using a Hitachi S-800 field emission scanning electron microscope operating at a 25 kV acceleration voltage. Sol−gel-derived films were overcoated with a 20 nm layer of evaporated carbon to maintain surface-charge continuity.

Profilometry. Film thicknesses were determined using a Tencor Instruments Alpha-step 500 profilometer with a diamond-point stylus. Triplicate samples of each film type were measured. The film thicknesses reported represent the average and associated standard deviations. An uncoated section of substrate, obtained by placing Scotch tape across the substrate edge prior to film deposition, was used as a baseline.

Electron Spectroscopy for Chemical Analysis (ESCA). ESCA spectra were obtained using a Physical Electronics Laboratories (PHI) Model 5100 spectrometer equipped with a Mg/Ti dual-anode source, an Al/Be window, a hemispherical analyzer, and single-channel channeltron detector. An achromatic Mg Kα X-ray (1253.6 eV) source was operated at 300 W, 15 kV, and 20 mA. The system base pressure was no higher than 2 × 10^{-8} Torr, with an operating pressure that did not exceed 1 × 10^{-7} Torr. A pass energy of 89.45 eV was used to obtain the survey spectra and 35.75 eV was used for the high-resolution, multiregion scans. Spectra were obtained at 15, 45, and 80° takeoff angles. The instrument was calibrated using Mg Kα X-radiation such that the Ag $3d_{5/2}$ peak of sputtered clean Ag had a binding energy of 367.9 ± 0.1 eV and the binding energy difference between the Cu $2p_{3/2}$ and Au $4f_{7/2}$ was 848.7 ± 0.1 eV. The full width at half-maximum for the Ag $3d_{5/2}$ peak was 0.80 eV at 30 000 counts/s. Data manipulation was performed using a Perkin-Elmer 7500 professional computer running PHI ESCA Version 2.0 software.

Diffuse-Reflectance Infrared Fourier Transform Spectroscopy (DRIFTS). DRIFT spectra were recorded with a Perkin-Elmer 1760X FT-IR spectrometer using a commercial diffuse-reflectance attachment and a liquid N_2 cooled MCT detector. All film spectra were blank corrected using a clean, uncoated substrate. IR spectra are the average of 1000 scans at 4 cm^{-1} resolution. The sample chamber was purged with dry N_2 before, between, and during each scan to minimize contributions from atmospheric water.

Fluorescence Spectroscopy. Steady-state fluorescence measurements were performed using an SLM 48000 MHF spectrofluorometer and an argon-ion (λ_{ex} = 488.0 nm) or He−Cd (λ_{ex} = 325 nm) laser as the excitation source. Emission spectra were all background subtracted and corrected for detector and monochromator nonlinearities. The bulk of the instrumentation has been described in detail elsewhere.[7,25,27] The emission spectral band-pass was 1 nm for the pyrene-doped films and 8 nm for all other films. For the O_2 sensing experiments, a 345 nm long-pass filter was used to collect all emission from the pyrene-doped sol−gel-processed films.

(27) Narang, U.; Jordan, J. D.; Bright, F. V.; Prasad, P. N. *J. Phys. Chem.* **1994**, *98*, 8101.

Results and Discussion

Scanning Electron Microscopy (SEM). Figures 1 and 2 present typical SEM images of TEOS- and TrEOS−C_8-derived sol−gel-processed films, respectively. The upper image within each panel pair corresponds to 100× magnification, while the lower panel pair image represents 1000× magnification of the area within the highlighted rectangle shown in the upper images. These SEM images illustrate several key points. First, the ultrasonic aerosol deposition method yields less cracked TEOS-derived films when compared to the spin-cast films (compare Figures 1A and 1C to 1B and 1D) even though the films were produced from the exact same sol−gel processing solution. (Cracking of these spin cast films can be completely eliminated by diluting the stock solution with alcohol;[3] however, the final films are thinner.) Second, conventional spin casting yielded highly rippled TrEOS−C_8-derived films (Figure 2B) that were very often cracked. This problem could also be eliminated by dilution of the stock solution with alcohol, but the final films were very thin. Third, the ultrasonic aerosol technique yielded more uniform TrEOS−C_8-derived sol−gel-based films (Figure 2A) that contained the organic (C_8) residue. Finally, aerosol-deposited TrEOS−C_8-derived films were characterized by small (diameter = 6 μm), raised, circular domains (blisters) dispersed randomly within an uncracked, unrippled film base.

Prior to comparing films prepared with TEOS:water molar ratios of 1:2 and 1:4, it is prudent to review the effects of alkoxide/water molar ratio on the sol−gel processing chemistry. It is well-known that the alkoxide/water molar ratio influences the final composite in at least three ways.[1−5] The first is by promotion of alkoxide hydrolysis, demonstrated first by Pouxviel and co-workers.[28] Second, for alkoxide/water molar ratios greater than 1/4, the alcohol producing condensation reaction is favored, while the water forming condensation reaction is favored when the molar alkoxide/water ratio is less than 1/4.[29] Third, excess water (above that needed for complete alkoxide hydrolysis) also promotes hydrolytic depolymerization (i.e., the reverse of the water condensation reaction).[29] The latter point is apparently important when one compares the SEM images of aerosol-generated sol−gel-derived films prepared with alkoxide:water molar ratios of 1:2 and 1:4 (compare Figures 1A and 1C). Aerosol deposition of the TEOS films were similar in many regards; however, the films prepared with a TEOS/water molar ratio of 1:4 always exhibited a greater fraction of particulates (Figure 1C). These particulates are likely associated with the aforementioned hydrolytic depolymerization process.[29]

Profilometry. Film thicknesses were measured for the TEOS- and TrEOS−C_8-derived samples (Table 1). The TEOS:water and TrEOS−C_8:water molar ratios were 1:2 and 1:3, respectively, for the films investigated. TEOS-based films produced using the aerosol deposition scheme (Table 1, "one application") were 0.62 ± 0.05 μm thick. Films produced using five successive applications (Table 1, "five applications") were 3.0 ± 0.02 μm thick. SEM images of these thicker TEOS-derived films (data not shown) were indistinguishable from those presented in Figure 1A. This result demonstrates that at least 3 μm thick, uncracked films can be quickly formed using successive aerosol-deposited layers one atop the other. Interestingly, the film thickness uniformity apparently improves with the number of aerosol coatings. This is consistent with subsequent film layers filling in defects or irregularities present in the lower film layers. The ultrasonic aerosol-deposition scheme also provides an attractive means to produce uniform sol−gel-derived films with tunable thicknesses. Spin coating of the exact same TEOS sol−gel processing solutions always resulted in the formation of 2.0 ± 0.10 μm thick films that were cracked (Figure 1B). Of course, one can easily form uncracked films via spin coating,[3] but they are thin.

Table 1. Summary of Profilometry Data for TEOS- and TrEOS−C_8-Derived Films[a]

sample	film thickness (μm)[a]
TEOS (one application)[b]	0.62 ± 0.05
TEOS (five applications)[b]	3.00 ± 0.02
TEOS[c]	2.00 ± 0.10
TrEOS−C_8[b]	0.70 ± 0.08
TrEOS−C_8[c]	2.00 ± 0.15

[a] Average ± standard devitation, resulting from at least three replicates. [b] Aerosol-generated films. [c] Films produced by spin coating.

The deposition scheme used also affected the thickness and morphology of the TrEOS−C_8-derived films. Aerosol-generated TrEOS−C_8 films produced by a single application were 0.70 ± 0.08 μm thick. Spin coating of the same stock solution yielded films that were 2.0 ± 0.15 μm thick. SEM images (Figure 2) revealed a few blisters on the aerosol-generated TrEOS−C_8 films. Spin coating lead to highly rippled, nonuniform films. The increased heterogeneity in the TrEOS−C_8-derived sol−gel processed films, relative to the TEOS samples, is fully consistent with our profilometry results. We speculate that the blisters formed in the TrEOS−C_8-derived sol−gel-processed films arise from a combination of the unfavorable interactions between the C_8 and the alcohol and water used in the sol−gel process and the evaporation of the alcohol and water that "freezes in" the blisters. No evidence of blisters were seen in the spin cast films even when the stock solution was dilution with EtOH.

Electron Spectroscopy for Chemical Analysis (ESCA). To minimize surface contamination from adventitious carbon, we prepared and aged a series of films under argon using the ultrasonic aerosol (five coats) and spin coating (one coat) schemes. An inert atmosphere sample-transfer vessel was used to transport the films from the glovebag directly to the ESCA instrument's ultrahigh vacuum environment. Takeoff angles (angle between the surface plane and the detector) of 15, 45, and 80° were used to control the sampling depth in the ESCA experiment. Table 2 (top section) provides estimated sampling depths for the C(1s), O(1s), and Si(2p) photoelectrons.[30]

Aerosol and spin cast films were prepared from the exact same sol−gel-processed stock solutions within

(28) Pouxviel, J. C.; Boilot, J. P.; Beloeil, J. C.; Lallemand, J. Y. *J. Non-Cryst. Solids* **1987**, *89*, 345.
(29) Brinker, C. J. *J. Non-Cryst. Solids* **1988**, *100*, 31.
(30) Seah, M. P.; Dench, W. A. *Surface Interface Anal.* **1979**, *1*, 2.

Table 2. ESCA Results for TEOS- (1:2) and TrEOS−C_8-Derived (1:3) Films[a]

element (photoelectron)	estimated sampling depths (Å)[b] 15°	45°	80°
C (1s)	12	33	46
O (1s)	10	28	40
Si (2p)	13	36	50

takeoff angle (deg)	TEOS/aerosol % C	% O	% Si	TEOS/spin cast % C	% O	% Si
15	33.5 ± 0.1	49.1 ± 0.05	17.5 ± 0.05	28.1 ± 0.05	53.3 ± 0.02	18.6 ± 0.05
45	28.6 ± 0.2	52.5 ± 0.2	18.9 ± 0.02	22.6 ± 0.6	56.9 ± 0.5	20.6 ± 0.1
80	27.8 ± 0.7	53.1 ± 0.5	19.1 ± 0.2	19.9 ± 0.8	58.9 ± 0.7	21.2 ± 0.08

takeoff angle (deg)	TrEOS−C_8/aerosol % C	% O	% Si	TrEOS−C_8/spin cast % C	% O	% Si
15	66.3 ± 0.8	23.4 ± 0.9	10.3 ± 0.03	78.1 ± 0.03	14.0 ± 0.03	7.88 ± 0.02
45	45.9 ± 0.03	38.7 ± 0.2	15.4 ± 0.3	73.1 ± 0.3	18.1 ± 0.3	8.78 ± 0.05
80	41.7 ± 3	42.0 ± 2	16.4 ± 0.7	73.6 ± 0.1	17.5 ± 0.1	8.91 ± 0.01

[a] Average ± standard deviation, resulting from at least three replicates. [b] Estimated using equations from ref 30.

5−10 min of one another and films were prepared in a random sequence. The aerosol and spin coating apparati were also contained within the exact same argon-purged atmosphere environment at the same temperature, and all samples were handled exactly the same. Thus, film differences are unlikely to result from differences in the sol−gel processing solution, sample handling protocol, and/or deposition chamber environment.

The middle and lower sections of Table 2 present the elemental surface analytical data for TEOS-derived films produced using the aerosol and spin-coating film generation methods (molar TEOS:water = 1:2). Analysis of dip-coated sol−gel-derived films that have been anneled between 100 and 500 °C have been reported.[31] In an ideal case, a completely hydrolyzed TEOS-based sol−gel-derived composite, free of adsorbed carbon contaminants, would exhibit no detectable carbon signal in the ESCA spectra. ESCA spectra for all our TEOS films reveal that carbon is always present at the surface, and the %C decreases as the sampling depth increases. Further, approximately 6% more carbon is reproducibly observed (95% confidence level) at all sampling depth for the aerosol-generated films relative to the spin-cast films.

Carbon present on the surface of the TEOS-derived samples is consistent with the presence of residual interfacial ethoxide units associated with incomplete hydrolysis of the metal alkoxide precursor during sol−gel processing. (It is also likely that a portion of the observed carbon signal arises from unavoidable carbon-containing contaminants.) However, the reproducible difference between %C on the surface (12 Å) of the aerosol-generated and spin-cast (34 vs 28%) films suggests that certain aspects of the final sol−gel-derived films can actually be manipulated by the choice of film-formation method. Specifically, these ESCA results suggest that the extent of ethoxide hydrolysis is lower at the top 10−50 Å of the aerosol-derived films compared to those produced by spin coating. Also, a more carbon rich 10−50 Å top surface can apparently be produced using TEOS and the aerosol deposition scheme. This result suggests that the sol−gel-processed droplets that impinge on the substrate to form the aerosol-derived film pick up more contaminates at their surface between the time they are produced and they impact the substrate and/or the extent of hydrolysis at the surface of these droplets is less compared to the surface of a spin-cast film. If the latter is true, this suggests that one can control the hydrolysis by controlling the actual droplet size. This issue is currently being explored in our laboratories.

Table 2 also summarizes the ESCA data for TrEOS−C_8-derived films produced using the aerosol and spin coating schemes (molar TrEOS−C_8:water = 1:3). These results illustrate several interesting aspects that merit additional discussion. First, the %C present in all the TrEOS−C_8-derived films is as expected significantly higher compared to the TEOS-derived films. Second, the TrEOS−C_8-derived sol−gel-processed films produced by spin-coating exhibit statistically higher %C values for all sampling depths relative to the films prepared using the aerosol method. (This is to be contrasted with the TEOS results.) Third, carbon appears more uniformly distributed (over the upper 10−50 Å) within the spin-coated TrEOS−C_8-derived films, with the %C varying only 5−6% between the top 10 Å to top 30−50 Å of the film. In contrast, the aerosol-generated films exhibited over 25% greater carbon at the top 10 Å of the film relative to carbon level detected up to 50 Å from the surface. These data clearly indicate segregation, on a 50 Å scale, for the organic residue within the TrEOS−C_8-derived sol−gel-processed films that have been produced using the aerosol generation method. We propose that there is a C_8-rich region in the topmost layer of the TrEOS−C_8-derived sol−gel-processed films that is due in part to segregated C_8 hydrocarbon chains in the outermost portion of the sol−gel-derived film.

These results are consistent with the distribution of carbon containing residues within an aerosol droplet being significantly different than the bulk distribution in solution and/or significant differences in the dynamics of C_8 unit within a droplet on impact with the substrate surface compared to a spin-cast film at the substrate surface. That is, if the C_8 residues are distributed differently within a droplet compared to the bulk, it is

(31) Santucci, S.; DiNardo, S.; Lozzi, L.; Passacantando, M.; Picozzi, M. *J. Electron. Spectrosc. Rel. Phenom.* **1995**, *76*, 623.

reasonable to expect the C_8 residue distribution at the surface of the droplet on impact with the substrate to be different from the results seen from a film produced by bulk casting. If this scenario were in operation, it would suggest that our aerosol-derived droplets are inherently much more heterogeneous, in terms of their compositional distribution, than the bulk solution. Complex distribution patterns are the norm in reverse micelle systems[32] that have features akin to the C_8-based ORMOSIL. In the other scenario, if the C_8 residue dynamics/solvation are different during the progression that leads to film formation, then one would expect differences in the distribution of C_8 residues within the final film. If this scenario were to operate, our results suggest that the C_8 residue within the top 10−50 Å of the spin-cast films are dynamical enough that during the film formation event the C_8 residues redistribute themselves more or less randomly throughout the top 50 Å of the film (there may be some segregation in the top 10−30 Å of the spin-cast film, but this is not as clear-cut as in the aerosol-deposited films). In the aerosol-deposited films, such a dynamical scenario suggests that the C_8 residue dynamics are not fast enough to allow for redistribution during the film-formation event, and the distribution/segregation becomes frozen in.

DRIFTS. In the previous section, ESCA revealed that statistically greater carbon levels were present at the surface of the TrEOS−C_8 spin-cast films relative to the aerosol-generated specimens and that there was segregation of the organic carbon residues at the aerosol-generated TrEOS−C_8-derived sol−gel-processed films. These results are intriguing, given that the films were prepared from the exact same stock solution and formed in the exact same environment.

Diffuse-reflectance infrared Fourier transform spectroscopy (DRIFTS) is a well-established technique for qualitative and quantitative analysis of powders, turbid liquids, and coatings that scatter to a high degree.[33,34] We used DRIFTS to estimate if hydrolysis within the films had gone to completion and to qualitatively compare the bulk carbon concentration within TrEOS−C_8 films produced from the aerosol and spin-coating methods. Analysis of the DRIFT spectra followed from previous work on sol−gel-derived silicates, *n*-alkyl ORMOSILS, and water.[35−41] DRIFT spectra (not shown) for the TEOS-derived films exhibited no detectable asymmetric stretch for chain methylene (ca. 2925 cm^{-1}), symmetric stretch for $-CH_3$ (ca. 2890 cm^{-1}), or $-O-CH_3$ (ca. 2838 cm^{-1}). The $-CH_2-$ (2930−2921 cm^{-1}) and $-CH_3$ (2884−2880 cm^{-1}) modes were readily observed in the TEOS and TrEOS−C_8 precursor DRIFT spectra. The TrEOS−C_8 film DRIFT spectra (molar TrEOS−C_8:water = 1:3) exhibited strong C−H stretching in the 2925 and 2890 cm^{-1} regions that were independent of the film production method. These results are consistent with hydrolysis going to completion within the TEOS- and TrEOS−C_8-derived films. (Note: it is unlikely that the DRIFTS technique could identify a few percent or less of unhydrolyzed materials in these films especially if such were localized to the top 50 Å of the film.) These results also suggest that there is little if any detectable difference in the *bulk* alkyl content within the TrEOS−C_8-drived films regardless of the preparation methodology. These results may appear to contradict our ESCA results; however, any differences are likely a result of the ESCA sampling only the topmost 50 Å of the film whereas the DRIFTS essentially probes the entire film.

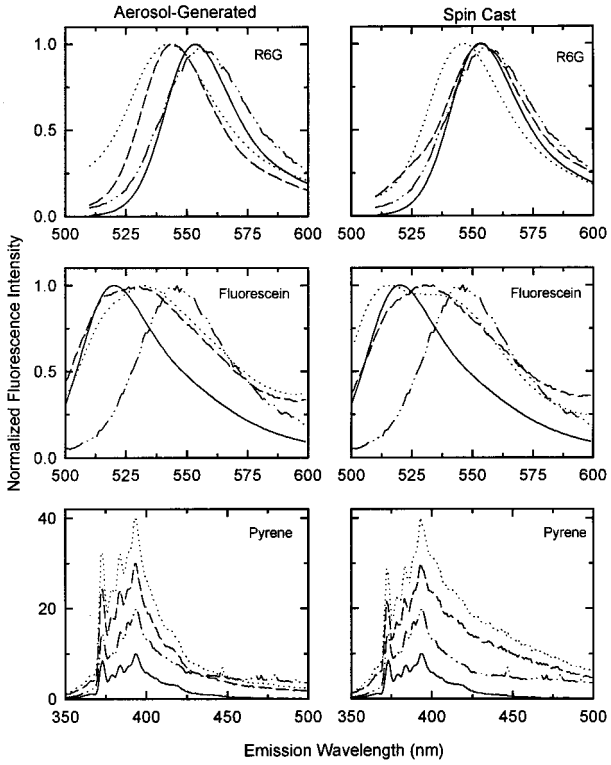

Figure 3. Emission spectra of R6G, fluorescein, and pyrene in ethanol (—), adsorbed to bare substrate (—••—), and entrapped within thin films produced from sol−gel solutions with TEOS:ethanol:water:HCl of 1:2:2:10^{-5} (- - - -) and 1:2:4:10^{-5} (•••) for aerosol-generated and spin-cast films, respectively.

Steady-State Fluorescence. The local microenvironment surrounding a series of model dopants (R6G, fluorescein, and pyrene) was determined by following their steady-state fluorescence. Typical emission spectra are presented in Figure 3 where the left-hand panels correspond to aerosol-generated films and the corresponding spin-cast films are shown in the right-hand panels. Shown within each individual panel set are the emission spectra for each dopant/probe in neat liquid ethanol (—), the probe adsorbed to the bare substrate (—••—), and the probe entrapped within films produced from sol−gel-processed solutions with TEOS:ethanol:water:HCl of 1:2:2:10^{-5} (- - - -) and 1:2:4:10^{-5} (•••).

(32) Luisi, P. L. *Angew. Chem., Int. Ed. Eng.* **1985**, *24*, 439.
(33) Krishnan, K.; Ferraro, J. R. In *Fourier Transform Infrared Spectroscopy: Techniques Using Fourier Transform Interferometry*; Ferraro, J. R., Basile, L. J., Eds.; Academic Press: New York, 1982; Vol. 3, Chapter 5.
(34) Boroumand, F.; van den Bergh, H.; Moser, J. E. *Anal. Chem.* **1994**, *66*, 2260.
(35) Bayly, J. G.; Kartha, V. B.; Stevens, W. H. *Infrared Phys.* **1963**, *3*, 211.
(36) Orcel, G.; Phalippou, Hench, L. L. *J. Non-Cryst. Solids* **1986**, *88*, 114.
(37) Perry, C. C.; Li, X. *J. Chem. Soc., Faraday Trans.* **1991**, *87*, 761.
(38) Perry, C. C.; Li, X. *J. Chem. Soc., Faraday Trans.* **1991**, *87*, 3857.
(39) Capozzi, C. A.; Pye, L. D.; Condrate, R. A. *Mater. Lett.* **1992**, *15*, 130.
(40) Capozzi, C. A.; Condrate, R. A.; Pye, L. D.; Hapanowicz, R. P. *Mater. Lett.* **1994**, *15*, 349.
(41) Ou, D. L.; Seddon, A. B. *J. Non-Cryst. Solids* **1997**, *210*, 187.

We turn first to the R6G-doped films. It is well-known that the R6G fluorescence is generally insensitive to the physicochemical properties of its local environment.[42−46] However, the R6G emission profile is sensitive to the extent of R6G intermolecular association.[42,47,48] In previous work from this group[48] a 16 nm blue shift was observed for R6G within sol−gel-derived films if the probe concentration exceeded 50 μM. Early work by Reisfeld and co-workers[47] and our more recent work[48] also demonstrate that R6G entrapment within a sol−gel-processed composite generally decreases the extent of R6G aggregation relative to the level seen in an aqueous solution at similar R6G concentrations. Thus, the blue shift observed for the R6G-doped sol−gel-processed films is consistent with some degree of R6G aggregation within these films. The extent of the R6G aggregation appears to be more prevalent in the aerosol-generated films compared to the spin-cast films. This result suggests that the distribution of R6G molecules within the aerosol droplet is such that the R6G molecules are closer together than in the spin-cast film. This would be consistent with the proposed compositional heterogeneity of these droplets described above.

In solution, fluorescein can exist as a cation, neutral, anion, and dianion.[49] Only the neutral, anion, and dianion are excited under our experimental conditions, and only the anion and dianion fluoresce. In ethanol we see an emission spectrum much akin to the fluorescein dianion. When fluorescein adsorbs to a silanol-rich interface, the fluorescence spectrum is red shifted by 35 nm. The fluorescence spectrum from fluorescein within the sol−gel-processed films is significantly broader than its emission in either ethanol or adsorbed at the glass surface. This result is consistent with simultaneous emission from more than one form of fluorescein.

Kubista and co-workers[49] have carefully characterized fluorescein's proteolytic equilibria in aqueous solution and determined the spectroscopic properties of the individual emissive species in solution. Specifically, the authors found that the fluorescein dianion emits maximally between 510 and 515 nm. In solution the anion has a lower quantum yield compared to the dianion with two peaks—one near 510−515 nm and a second shoulder near 550 nm. Our spectra for fluorescein entrapped within the sol−gel-processed films are more in line with the presence of both the anion *and* the dianion. In this case, the degree of heterogeneity surrounding the fluorescein is apparently greatest for the spin-cast films.

These results are consistent with the fluorescein molecules locating simultaneously between two or more microdomains within the sol−gel-derived flims. One of the microdomains is such that the fluorescein anion is formed and the other microdomain (the one with the more basic sites/residues) supports the dianionic species. The relative magnitude of the two forms is a qualitative measure of the occupation of these individual microdomains by fluorescein and/or the heterogeneity of the environment surround the fluorescein molecules.

Table 3. I_1/I_3 Values for Pyrene Molecules Entrapped within and Adsorbed to Various Sol−Gel-Derived Thin Films[a]

Sol−Gel-Derived Film Entrapped Pyrene		
TEOS:water molar ratio	TEOS/aerosol	TEOS/spin cast
pyrene in ethanol	1.10 ± 0.01	1.10 ± 0.01
1:2	1.16 ± 0.04	0.789 ± 0.03
1:4	1.19 ± 0.04	0.960 ± 0.04
Pyrene Adsorbed to Sol−Gel-Derived Films		
TEOS:water molar ratio	TEOS/aerosol	TEOS/spin cast
1:2	0.973 ± 0.04	0.869 ± 0.03
1:4	1.01 ± 0.05	0.875 ± 0.04
pyrene adsorbed to clean silica	0.852 ± 0.04	0.852 ± 0.04
TrEOS−C_8:water molar ratio	TrEOS−C_8/aerosol	TrEOS−C_8/spin cast
1:3	0.640 ± 0.01	0.607 ± 0.03

[a] Average ± standard deviation, resulting from at least three replicates.

Emission spectra from the pyrene-doped sol−gel-derived films are shown in the lower panels of Figure 3. The pyrene emission spectra possess several well-defined vibronic bands between 370 and 410 nm. The intensity ratio of the I_1 to I_3 peaks (I_1/I_3) provides an empirical measure of the physicochemical properties surrounding the average pyrene molecule.[50−59] For example, the pyrene I_1/I_3 is 0.41 in the gas phase and it is 1.95 in liquid dimethyl sulfoxide.[52] Thus, I_1/I_3 values yield a convenient measure of the average dipolarity surrounding the pyrene molecule. The I_1/I_3 values for pyrene entrapped within or adsorbed to the various sol−gel-derived film types are presented in Table 3. These data illustrate how the choice of deposition method influences the local physicochemical properties surrounding the average pyrene dopant.

Inspection of the pyrene I_1/I_3 data (Table 3) reveals several interesting trends. First, the I_1/I_3 values for pyrene molecules entrapped within the aerosol-generated TEOS films are in all cases significantly greater (99% confidence level) compared to pyrene molecules sequestered in a spin-cast film but are reasonably close to the I_1/I_3 value for pyrene in neat liquid ethanol. This

(42) Oh, H. T.; Kam, H.-S.; Kwon, T. Y.; Moon, B. K.; Yun, S. I. *Mater. Lett.* **1992**, *13*, 1139.
(43) Knobbe, E. T.; Dunn, B.; Fuqua, P. D.; Nishida, F. *Appl. Opt.* **1990**, *29*, 2729.
(44) Avnir, D.; Kaufman, V. R.; Reisfield, R. *J. Non-Cryst. Solids* **1985**, *74*, 395.
(45) Reisfield, R.; Eyal, M.; Brusilovsky, D. *Chem. Phys. Lett.* **1988**, *153*, 210.
(46) Kobayashi, Y.; Kurokawa, Y.; Imai, Y.; Muto, S. *J. Non-Cryst. Solids* **1988**, *105*, 198.
(47) Avnir, D. Levy, D.; Resifeld, R. *J. Phys. Chem.* **1984**, *88*, 5956.
(48) Narang, U.; Bright, F. V.; Prasad, P. N *Appl. Spectrosc.* **1993**, *47*, 229.
(49) Sjöback, R.; Nygren, J.; Kubista, M. *Spectrochim. Acta Part A* **1995**, *51*, L7.
(50) Dunbar, R. A.; Jordan, J. D.; Bright, F. V. *Anal. Chem.* **1996**, *68*, 604.
(51) Birks, J. B. *Photophysics of Aromatic Molecules*; Wiley-Interscience: New York, 1970.
(52) Dong, D. C.; Winnik, M. A. *Can. J. Chem.* **1984**, *62*, 2560.
(53) Dong, D. C.; Winnik, M. A. *Photochem. Photobiol.* **1982**, *35*, 17.
(54) Ham, J. S. *J. Chem. Phys.* **1953**, *21*, 756.
(55) Lochmüller, C. H.; Wenzel, T. J. *J. Phys. Chem.* **1990**, *94*, 4230.
(56) Winnik, F. *Chem. Rev.* **1993**, *93*, 587.
(57) Li, M.; Pacholski, M. L.; Bright, F. V. *Appl. Spectrosc.* **1994**, *48*, 630.
(58) Samuel, J.; Polevaya, Y.; Ottolenghi, M.; Avnir, D. *Chem. Mater.* **1994**, *6*, 1457.
(59) Kaufman, V. R.; Avnir, D. *Langmuir* **1986**, *2*, 717.

suggests that the average local microenvironment surrounding pyrene in the aerosol-derived TEOS films is more dipolar compared to films spin cast from identical stock solutions. This implies that more dipolar residues/species surround the average pyrene molecule in the aerosol-derived films vs the spin cast films. Second, the I_1/I_3 for pyrene entrapped within the 1:2 TEOS-derived spin-cast films is statistically less (99% confidence level) than the value seen for pyrene adsorbed to the bare silica substrate. This is consistent with a much less dipolar environment within the 1:2 TEOS spin-cast film than is encountered at a clean silica surface. This might result from the presence of a greater number of less polar O−Et residues (relative to Si−OH) surrounding the pyrene in the 1:2 TEOS spin-cast film. Third, the I_1/I_3 for pyrene molecules sequestered within the 1:4 TEOS spin-cast films is statistically less (99% confidence level) than the value for the aerosol-generated TEOS film derived from the same sol−gel-processed solution. Again, the dipolarity within the aerosol-deposited film is much greater than the spin-cast film. Fourth, there is no clear statistically significant difference, as sensed by pyrene, between the 1:2 and 1:4 TEOS-based films that have been produced by the aerosol-generation method. This demonstrates that the microdomain surrounding the average pyrene molecule within the aerosol-generated films remains at a relatively high dipolarity regardless of the initial water level used in the sol−gel-processed solution. Interestingly, the dipolarity sensed by pyrene within the aerosol-based film (i.e., $I_1/I_3 = 1.16-1.19$) is also slightly greater than that of neat liquid ethanol ($I_1/I_3 = 1.10$). This could arise from the combined effect of residual solvent and silanol groups.

Our ESCA results suggested surface segregation of carbon in several of the film types investigated. Clear, statistical differences in the relative %C levels (see Table 2) were also observed between aerosol-generated and spin-cast films prepared from identical sol−gel-processed stock solutions. Differences of this sort in the film surface carbon coverage should also affect the film interfacial dipolarity and thus influence the physicochemical properties and intermolecular interactions that occur at the film surface. To investigate this issue in more detail, neat sol−gel-processed films were prepared as described above and incubated in 0.5 μM pyrene solutions (in ethanol) for 1 h, the films were rinsed with ethanol, and they were allowed to dry. The emission spectra from the adsorbed pyrene molecules were then acquired (data not shown), and I_1/I_3 was recorded (Table 3). For comparison, the I_1/I_3 value for pyrene adsorbed to a dry, low-porosity, bare fused-silica substrate is also reported (0.852 ± 0.04).

Inspection of the adsorbed pyrene emission results show that the TrEOS−C_8-derived film surfaces are significantly (99% confidence level) less dipolar when compared to bare silica or a TEOS-derived sol−gel-processed film (1:2 or 1:4). This result indicates that the pyrene molecules adsorbing to the TrEOS−C_8-derived films are encountering a statistically less dipolar microdomain at the surface and pores of the TrEOS−C_8-derived films. This conclusion is fully consistent with the ESCA data, demonstrating that the spin-cast TrEOS−C_8-derived films exhibited a 12% greater carbon level at the surface relative to the aerosol-generated films (Table 2). The results are also in line with recent chromatographic results.[19a] The adsorbed pyrene data also reveal that the dipolarity of all film surfaces is generally lower than the corresponding bulk films. Again, this is consistent with the ESCA results wherein carbon was segregated at the surface of all film types.

One apparent inconsistency between our surface fluorescence and ESCA data lies in the comparison of the aerosol and spin-cast TEOS films. Specifically, in the ESCA experiments we found that the %C at the surface was statistically greatest for the aerosol-derived films vs the spin-cast films (Table 2). Given this, we would predict the I_1/I_3 value for pyrene "adsorbed" to the aerosol-derived film to be less than the spin-cast films. Inspection of Table 3 shows the reverse to be true. One explanation for this discrepancy is associated with the porosity of the sol−gel-processed materials.[1−5]

In our ESCA experiments one probes only the topmost 50 Å of the film and not an appreciable amount of interstitial surface (e.g., pores). In our "interfacial" fluorescence experiments that use pyrene, the probe can distribute itself at all accessible surfaces associated with the entire film because the film is porous.[1−5] That is, the pyrene molecules can locate simultaneously at regions of the film that one can study by ESCA as well as at the surface of some pores more deep within the film structure that cannot be accessed by the ESCA experiment. If the dipolarity of these pores were greater than the surface that one can access in an ESCA experiment and there is a population of the pyrene molecules associated with these pore surfaces, then one would actually observe a collective I_1/I_3 value for adsorbed pyrene that can be inconsistent with the %C from the ESCA experiments depending on how dipolar the pore is relative to the surface proper and the distribution coefficient for the pyrene between the ESCA-accessible surface and the ESCA-inaccessible pore surface.

It is well-known that the pyrene fluorescence can be effectively quenched by O_2.[50−59] As a result, one can exploit the pyrene (Py) fluorescence to obtain information on the efficiency of O_2 quenching ($Py^* + O_2 \rightarrow Py + O_2$) *and* estimate the accessibility of the pyrene molecules sequestered within the sol−gel-processed films to the quencher/analyte.[60]

In previous work from one of our groups,[50] the pyrene/O_2 system was used to quantify the accessibility and stability of the "sensing chemistry" (i.e., pyrene) when it was entrapped within sol−gel-derived films that were produced by a dip-coating method. To estimate the potential of our aerosol-deposited sol−gel-derived thin films as sensing platforms, we carried out a limited set of experiments on aerosol-generated, spin-cast, and dip-cast films subjected to gaseous N_2 and O_2 atmospheres. The thicknesses of these films and the pyrene concentrations within the films were all within ±20%. The results of these experiments are presented in Figure 4. Several aspects of these results merit mention. First, pyrene molecules entrapped within the aerosol-deposited sol−gel-derived thin film (Figure 4A) are quenched by O_2. Second, the response times ($O_2 \rightarrow N_2$ and $N_2 \rightarrow O_2$) for an aerosol-based film are significantly less than 1 s.

(60) Lakowicz, J. R. *Principles of Fluorescence Spectroscopy*; Plenum Press: New York, 1983.

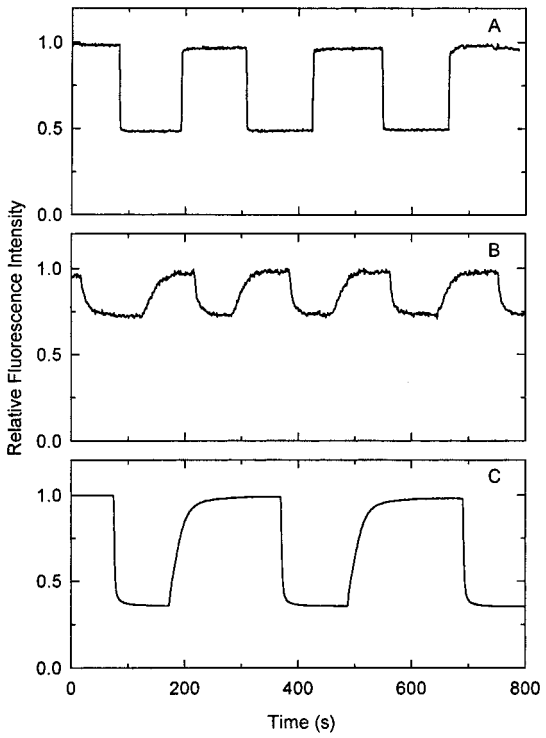

Figure 4. Fluorescence response of pyrene-doped sol−gel-derived films subjected to N_2 and O_2 atmospheres. Aerosol-generated (A) and spin-cast (B) thin films on quartz. Dip-cast film on the distal end on an optical fiber (C).

(Note: all response times are biased toward longer times by the time required to physically switch gases and purge the gas feed lines that lead to the optical cell.) Second, the aerosol-derived film response time is several-fold better when compared to the response times associated with the spin-cast (Figure 4B) and dip-cast sol−gel-derived films (Figure 4C). Third, the response for all three films is completely reversible. Fourth, the O_2 to N_2 response is at least 1 order of magnitude faster for the aerosol-generated films compared to the other film types (compare Figure 4A to Figures 4B and 4C). Finally, the best analytical response is observed from the dip-cast film followed next by the aerosol-derived film; the spin-cast film analytical response is clearly the most poor. These results are likely a result of a combination of factors including film porosity, relative distribution of the pyrene within the film pore structure, and the environment surrounding the pyrene molecules which modulates the excited-state pyrene lifetime.[50] These issues are under current investigation in our laboratories.

Air Brush Generated Films. We questioned if we could use alternative "spray" methods to produce sol−gel-derived films/coatings. In Figure 5 we present SEM images of TEOS-derived films (molar ratio of TEOS:ethanol:water:HCl $1:2:2:10^{-5}$) on borosilicate glass. These particular films were produced by simply using a commercially available arts and crafts model air brush (Badger). In Figure 5A the upper image represents a 100× image, while the lower image represents a 1000× magnification of the area within the highlighted rectangle shown in the upper image. Figure 5B illustrates a 3000× image of the tape edge between the glass substrate and the air brush generated, sol−gel-derived film. These results illustrate that one can use a simple, inexpensive air brush to deposit and form reasonable quality sol−gel-processed films. The films that are formed using the air brush are not yet as homogeneous as the films formed by our ultrasonic aerosol method, but they are clearly superior to our thicker films formed by the spin-coating method.

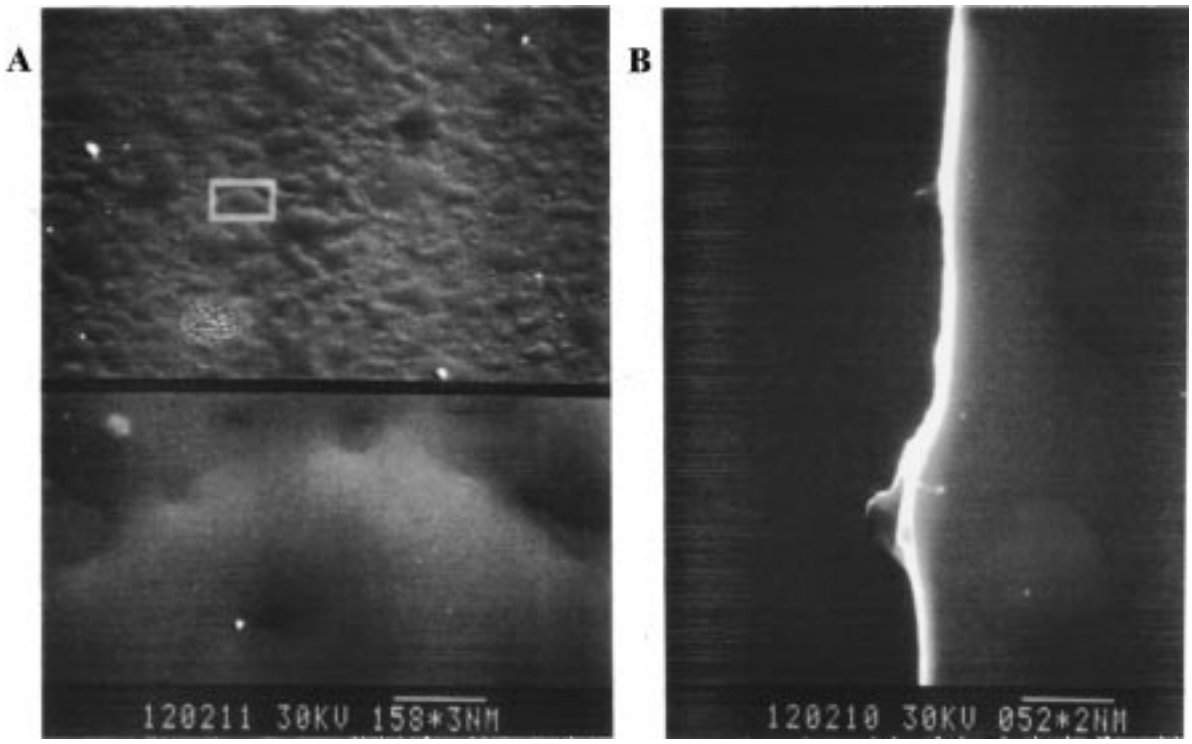

Figure 5. Scanning electron micrographs of TEOS-derived films produced using an air brush deposition method. Molar ratio of TEOS:ethanol:water:HCl::$1:2:2:10^{-5}$. (A) 100× magnification (upper), 1000× magnification (lower). The scale corresponds to the upper image. (B) 3000× magnification of the tape edge between the glass substrate and the TEOS-derived film coating.

Conclusions

We have developed an inexpensive, fast, and convenient method for producing uniform sol−gel-derived films under ambient conditions using ultrasonic or air-driven aerosol methods. We have compared TEOS- and TrEOS−C_8-derived sol−gel-processed films produced using the ultrasonic aerosol-generation method to those produced by a conventional spin-casting scheme.

SEM showed that aerosol-generated films were uniform, while spin casting, from identical sol−gel processing solutions, resulted in highly cracked films. Spin casting from TrEOS−C_8 sol−gel processing solutions produced films with a rippled, cracked surface. Aerosol generation, in contrast, yielded more uniform TrEOS−C_8-derived films, but these films had somewhat blistered surfaces. The thickness of the aerosol-generated films were between 0.6 and 0.7 μm for a one-step coating. The thickness of the corresponding spin-cast films were 2.0 μm. Five repetitive aerosol deposition steps led to uniform ($\pm$0.02 μm) 3.0−3.5 μm thick films that were uncracked. Thus, thicker uncracked sol−gel-derived films can be easily formed using the aerosol deposition approach.

ESCA results showed that the deposition method influenced the amount of carbon-containing species at the film surface. For the TrEOS−C_8-derived films, spin-cast films statistically exhibited greater carbon at the surface relative to the aerosol-generated films. The difference between %C at the topmost 10 Å and the topmost 50 Å was 25% for the aerosol-deposited films, while spin coating produced a more uniform carbon distribution, varying only 5% over the same sampling depths. Possible reasons for this difference included differences in the distribution and/or differences in the dynamics/solvation of the C_8 residue in the droplet vs the bulk sol−gel-processed solution. Regardless of the operating mechanism, with the ORMOSIL precursor, one's choice of film deposition method influences the final distribution of an organic moiety at the film interface. This point is of particular importance for situations such as those involving the use of ORMOSILs as a stationary phase for chromatographic and electrophoretic applications[19] and chemical sensing where issues of fouling and system compatibility are key.[6]

Static fluorescence spectroscopy showed that neutral, anionic, and cationic dopants can be incorporated directly into the sol−gel processing solution and deposited within films by using our aerosol-deposition method. These results all demonstrate that, from the perspective of these probe molecules, these films are heterogeneous on at least the scale of these probes. This is consistent with earlier work from one of our laboratories.[27] Results from adsorbed pyrene can only be explained only by considering that it distributes simultaneously between the surface proper and internal film pores. This illustrates a potential problem with attempting to use probes such as pyrene to probe the "surface" of highly porous materials.

Pyrene-doped, aerosol-generated film architectures exhibited reversible subsecond response times to gas-phase O_2, while response times for spin-coated films were on the order of 25 s. The performance from these thin films was also compared to previous work[50] in which pyrene-doped sol−gel-derived films were produced by dip coating the distal end of an optical fiber. In this case the aerosol-generated films were much superior in terms of response times. Response magnitudes are in all cases comparable.

Our aerosol-deposition scheme is also compatible with the immobilization of any chemical recognition element in a sol−gel-derived film architecture.[25] Finally, an advantage of this method, not exploited in the current work, is that the aerosol technique is not limited to coating regularly shaped substrates (e.g., plates, fibers).[26]

Acknowledgment. This work was generously supported by the National Science Foundation DMR-9303032 (to J.A.G.) and CHE-9626636 (to F.V.B.), the Office of Naval Research (to F.V.B.), and the Whitaker Foundation (to L.A.C.). We also thank Professor P. N. Prasad and his research team for allowing us access to their profilometer. *To whom all correspondence should be directed: 716-645-6800 ext. 2162 (voice), 716-645-6963 (FAX), chefvb@acsu.buffalo.edu (e-mail).

CM970612R